# Establishing a Pure Sample of Side-Piercing Through-Going Cosmic-Ray Muons for LArTPC Calibration in MicroBooNE
# MICROBOONE-NOTE-1028-PUB

**The MicroBooNE Collaboration**

07/22/17

### Abstract

Measuring detector properties and performing calibrations of a near-surface Liquid Argon Time Projection Chamber (LArTPC) require large samples of well-reconstructed tracks. Cosmic-ray muon tracks are an ideal calibration source for a surface TPC for these purposes, because they cover the detector volume roughly uniformly and enter the detector volume at a high rate. In order to calibrate the TPC's position response, the reconstructed track for the 3D trajectory of each cosmic-ray muon must be available. Because of the slow electron drift velocity, reconstructed track information along the drift-coordinate is offset with respect to the true energy deposition location. This offset can be corrected only if the time at which the track enters the detector volume ($t_0$) is also reconstructed. In this note we present a method developed for reconstructing track $t_0$ for the subset of cosmic-ray tracks which hit either the TPC anode-plane or cathode-plane and are through-going. Over 97% of the $t_0$-tagged tracks have their $t_0$ correctly reconstructed in both simuation in cosmic-ray data while maintaining yield values of 0.9 tracks per 4.8 ms exposure for cathode-piercing tracks and 1.7 tracks per 4.8 ms exposure for anode-piercing tracks in simulation. Coverage maps for an off-beam cosmic-ray data sample of $t_0$-tagged tracks produced with this method show that $t_0$-tagged track coverage is as expected given cosmic track geometries in the TPC, acceptance effects, and cut sensitivities.

## 1 Introduction

The MicroBooNE detector [1] is a near-surface, 170 ton Liquid Argon Time Projection Chamber (LArTPC) located 470 m along the Booster Neutrino Beamline (BNB) at Fermilab. The MicroBooNE detector observes neutrino interactions by means of three anode wire planes, 32 photomultiplier tubes, and timing information from the BNB. The MicroBooNE experiment is motivated by resolution of the MiniBooNE low-energy excess [2], performing novel measurements of neutrino cross sections on argon, and contributions toward LArTPC detector development, important for future searches of CP violation.

In MicroBooNE, track $y$ and $z$ coordinate information is reconstructed to millimeter resolution using the ionization electron signals deposited on the three wire planes [1]. There is ambiguity in the $x$ coordinate of the arriving tracks, which is offset by a constant proportional to the arrival time, $t_0$, at which the tracks arrive with respect to the zero of the data acquisition system. $t_0$ is defined as the track arrival time with respect to the recorded trigger time of each event. This quantity is needed for calibrations, which require full track position information.

This note presents an algorithm which reconstructs the $t_0$ of through-going cosmic-ray muons which enter or exit through the TPC anode-plane or cathode-plane. We describe the selection criteria applied to obtain a sample of $t_0$-tagged tracks with $\geq 97\%$ of tracks with correctly reconstructed $t_0$ in data and simulation. Further, we present $t_0$ reconstruction performance in this set. We display coverage maps with the trajectories of tracks with well-reconstructed $t_0$ across the detector, obtained employing this algorithm to off-beam (cosmic) data.

## 2 Algorithm Description

The MicroBooNE TPC boundaries are defined in a Cartesian coordinate system in which $x$, $y$, and $z$ denote the drift, vertical, and beam-aligned direction, respectively. Figure 1 shows a cartoon of the TPC which illustrates the coordinate system.
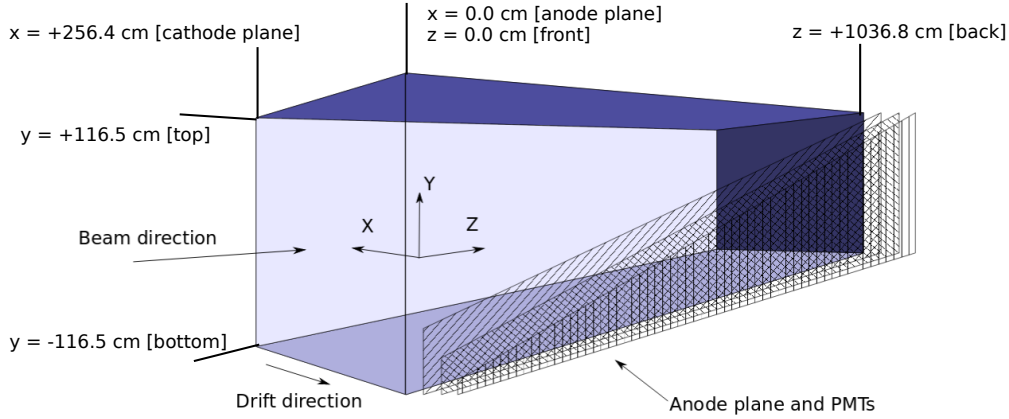
Figure 1: A cartoon depiction of the TPC coordinate system.

The algorithm for $t_0$ reconstruction makes the following assumptions about the tracks of cosmic-ray muons:

- The tracks are downwards-going.

- The tracks are through-going, meaning that they enter and exit the TPC.

The algorithm is designed to reconstruct track $t_0$ for muons which enter the top of the TPC and exit from either the anode or cathode, as well as tracks which enter from the anode or cathode and exit the bottom of the TPC. The algorithm currently ignores the case of tracks that enter or exit the TPC through the front-plane or back-plane but can be easily extended to include these cases. An example of a track that is $t_0$-tagged using this algorithm is depicted in Figure 2.

A reconstructed track is determined to enter or exit through the $y$ (top/bottom) or $z$ (front/back) TPC walls if either start-point or end-point is found to be within a distance $R$ of these detector boundaries. We choose a value of $R$ equal to 13 cm to fully account for any distortion in reconstructed track-position due to variations in the electric field across the TPC [3].

Under the assumption that cosmic muons are downward-going, the track end-point with the largest $y$ coordinate is taken to be the entering point. We determine a track to be entering or exiting the anode-plane or cathode-plane if either:
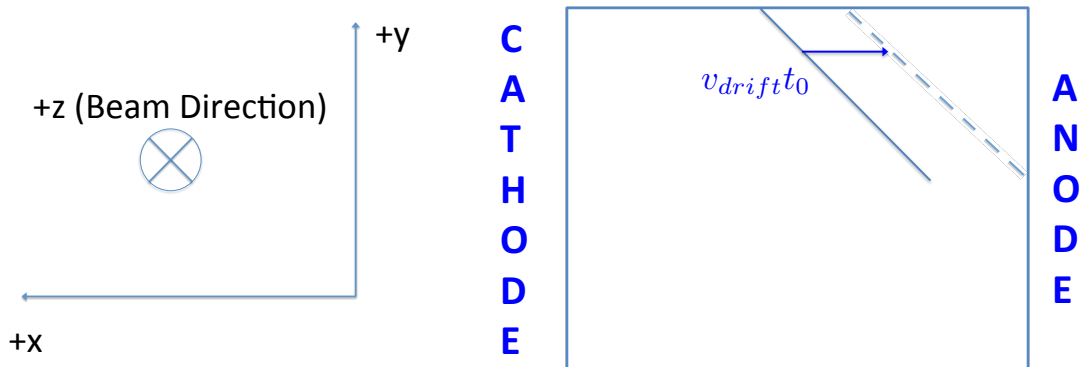


Figure 2: A schematic of an example side-piercing track $t_0$-tagged with this algorithm as shown for the $xy$ plane. This track enters the top of the TPC and exits through the anode. The solid line represents the reconstructed track and the dotted line represents the reconstructed track with the $t_0$ correction applied. This correction consists of a product of the drift velocity of electrons in liquid argon, $v_{drift}$, and reconstructed track $t_0$.

1. the entering point is found to enter from the top, and the exiting point is found not to exit through the bottom, front, or back of the TPC; or

2. the entering point is found not to enter from the top, front, or back, and the exiting point is found to exit from the bottom of the TPC.

The track is determined to be anode-piercing or cathode-piercing based on the $x$-coordinate values of its reconstructed endpoints. Because of the downwards-going assumption, if the $x$-coordinate of the end of the track is smaller than the entering $x$-coordinate, and the track enters from the top, the track pierces the anode-plane. The logic is inverted for tracks exiting the bottom of the TPC.

For anode-piercing tracks, charge associated with the anode-piercing $x$-coordinate $x_A$ will require no time to drift to the readout wires. Therefore, the $t_0$ can be reconstructed using the following equation in which $v_{\mathrm{drift}}$ is the drift velocity of electrons in liquid argon, approximately equal to 0.1114 cm/$\mu$s [4]:

$$t_0 = \frac{x_A}{v_{\mathrm{drift}}} \tag{1}$$

For cathode-piercing tracks, charge associated with the cathode-piercing $x$-coordinate $x_C$ will have to drift through the full TPC drift-length. Therefore, the $t_0$ value is given by the following equation in which $T_{\mathrm{drift}}$ is the time needed for ionization electrons to drift the full length of the TPC, approximately equal to 2300 $\mu$s [4]:

$$t_0 = \frac{x_C}{v_{\mathrm{drift}}} - T_{\mathrm{drift}} \tag{2}$$

In the above equations, both time and drift-distance are measured with respect to the event trigger time. Charge arriving at the anode-plane at the trigger-time will have a reconstructed $x$-coordinate of 0 cm.

Tracks which stop within the detector volume may mistakenly be tagged by the algorithm leading to an incorrectly reconstructed $t_0$. This is because the track end-point will be consistent with neither exiting from the bottom, nor the front or end of the TPC, and will therefore pass the selection cuts. Backgrounds in this category arise from stopping cosmic-ray muons and also broken tracks which should be through-going but are not fully reconstructed. Shorter tracks stitched together into longer ones can also result from reconstruction failures. In order to limit such backgrounds we rely on a simple matching of TPC and PMT information to determine if a track's $t_0$ was correctly reconstructed or not. Because scintillation light produced in the detector reaches the PMT system virtually instantaneously on the time scale of the track charge deposition measurements, each cosmic-ray muon will lead to a flash of light in the PMT system at time $t_0$. If no flash was recorded at a time in a given window around the reconstructed $t_0$, we assume the track's $t_0$ was reconstructed incorrectly and discard the track. The fact that we record sufficient pre-trigger and and post-trigger digitized charge data allows this technique to be executed.

# 3 Purity Studies

In this study, we measure the purity, the percentage of tracks that are truly anode-piercing or cathode-piercing, of a sample of tracks tagged by the $t_0$ reconstruction algorithm as we scan various parameters for both simulated events (for which truth information is available) and a sample of externally-tagged cosmic-ray muon data events [5]. The number and denomination of the tracks in each sample is shown in Table 1. Due to the orientation of the external cosmic-ray muon tagger, only cathode-piercing tracks are used in that sample for this analysis.

Table 1: The number of each type of side-piercing tracks in each sample used in the studies of purity and efficiency.

| Sample | Events | Total Tracks Passing Cuts | Anode-Piercing | Cathode-Piercing |
|---|---|---|---|---|
| Cosmics Simulation | 400 | 2119 | 1208 | 911 |
| Externally Tagged Data | 35724 | 10118 | 0 | 10118 |

## 3.1 Tunable Parameters

In order to enhance the purity of the selected tracks we scan over three parameters:

- the difference in time between reconstructed $t_0$ and a flash of scintillation light recorded by the PMTs (encapsulated in a quantity called the flash window, described in the next paragraph);

- the number of photoelectrons (NPEs) in the flash recorded by the PMTs; and

- the reconstructed track length ($L_{\text{track}}$).

A well-reconstructed $t_0$ should be well-correlated with the time of a flash recorded by the PMTs. The quantity which we use as purity-enhancing measure is the 'flash window': the maximum difference that the difference between the reconstructed $t_0$ and the time of a flash of scintillation light can have from the peak of that quantity for all tracks of the same side-piercing denomination. A through-going cosmic-ray muon typically induces flashes of tens to hundreds of PEs in the PMTs, so false side-piercing tracks would not satisfy this requirement. Stopping muon tracks tend to be shorter in length, so the cut on track length removes these tracks from consideration. A track length cut is also effective in removing broken tracks. The quantities that we use as a metric for each set of cuts are the purity and efficiency of the sample, defined as:

$$\text{Purity} = \frac{\text{Number of Tracks Passing Cuts With a Well-Reconstructed } t_0}{\text{Number of Tracks Passing Cuts}} \tag{3}$$

$$\text{Efficiency} = \frac{\text{Number of Tracks Passing Cuts}}{\text{Total Number of Tracks in Sample}} \tag{4}$$

Enacting these cuts enhances the purity of the sample while decreasing the yield of the sample. We wish to use a sample that exceeds the purity benchmark of 97% needed for calibration studies while keeping the yield as high as possible.

## 3.2 Simulation Sample

There are 400 events in the simulated sample. Cuts mandate that muon tracks in this sample must not be from BNB-induced events and must have 'truth' simulation information available. A reconstructed track is considered to have a well-reconstructed $t_0$ if the reconstructed $t_0$ is within a given range from the $t_0$ of the 'truth' track. This range is determined by the location and width of the peak of the ('Truth' Track $t_0$) - (Reconstructed Track $t_0$) quantity for all tracks piercing the same TPC side (the anode or cathode) in the simulated sample. This range is $\pm$ 4 $\mu$s from the peak for anode-piercing tracks and $\pm$ 8 $\mu$s for cathode-piercing tracks. Plots of this quantity for both anode-piercing and cathode-piercing tracks are shown in Fig. 3.
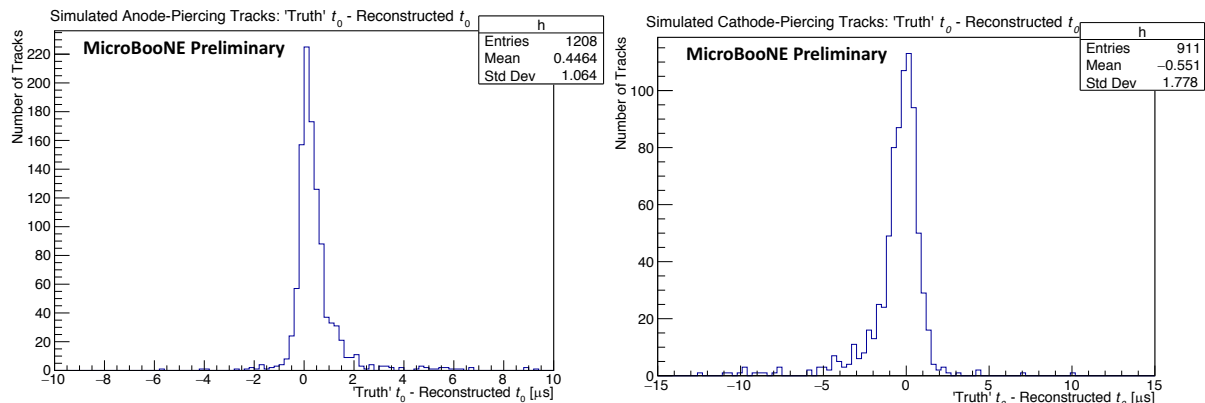


Figure 3: The distribution of the 'Truth' $t_0$ - Reconstructed $t_0$ difference for simulated anode-piercing (left) and cathode-piercing (right) tracks. Track $t_0$ is considered well-reconstructed if this quantity falls inside the range [-4 $\mu$s, 4 $\mu$s] for anode-piercing tracks and [-8 $\mu$s, 8 $\mu$s] for cathode-piercing tracks.

## 3.3 Externally Tagged Data Sample

There are 35,724 events in the externally tagged cosmic-ray sample. Tracks in these events are tagged by an external cosmic-ray tagger called the Muon Counter System (MuCS) which uses multiple scintillator strips to detect cosmic-ray muons and reconstruct their direction. This tagger, placed above the
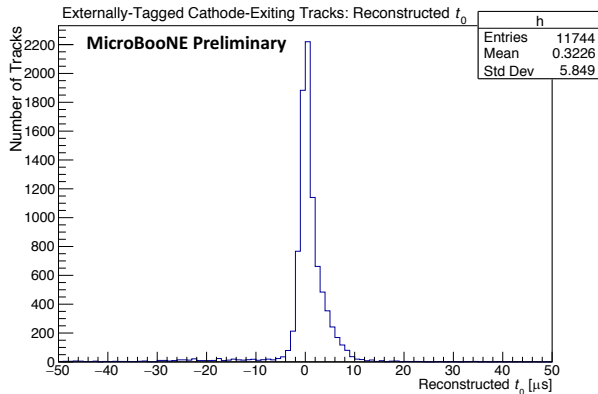
Figure 4: The distribution of the reconstructed $t_0$ distribution for the externally tagged muon tracks from data. Track $t_0$ is considered well-reconstructed if this quantity falls inside the range [-30 $\mu$s, 30 $\mu$s]. The only additional cut used to correct for the tagger impurities is that a track be cathode-piercing, hence the difference between entries in this plot and the number of tracks shown in Table 1.

MicroBooNE detector, can provide a trigger to the MicroBooNE DAQ. Events triggered by the MuCS will contain tracks which enter the TPC at the trigger-time ($t_0 = 0$ $\mu s$). We use these tracks to perform data-driven studies of $t_0$-tagging purity and efficiency. To limit the effect of inherent impurities on the external tagger, additional cuts are placed on the tracks tagged by this system. One of these cuts requires that a track be classified as top-entering, cathode-exiting by the algorithm, because the external muon tagger is oriented such that this denomination of track is likely to be the best-reconstructed. Information from these tracks constitute a reconstructed $t_0$ distribution sharply peaked near the zero of the data acquisition system, shown in Fig. 4. This is a product of the fact that these tracks trigger the events they are in and allows them to be used to validate this method in data. For our studies a well-reconstructed $t_0$ is one that falls within the range [-30 $\mu$s, 30 $\mu$s] from the zero of the data acquisition time, a value that is chosen to account for any distortions of track positions due to variations in the electric field [3] and other impurities in the TPC.

## 3.4 Scan Results

Here we display the results from scans of the cut parameters and values in the form of heatmaps. The $x$-axis displays the cut on track length [cm] and the $y$-axis displays the cut on the number of PEs required in a flash within the range specified at the top of the plot.

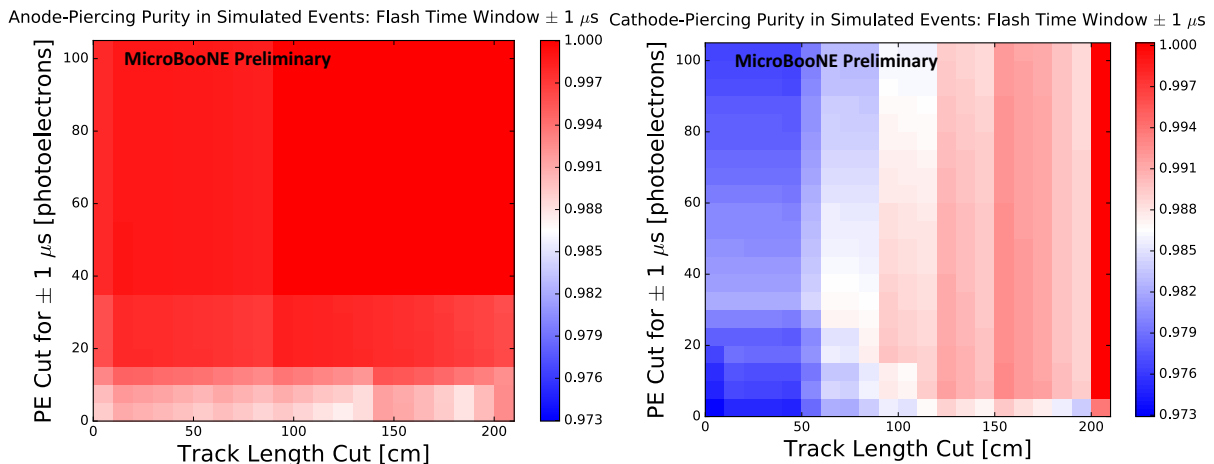In simulation we find that the anode-piercing sample maintains a higher purity than the cathode-



Figure 5: Heatmaps for the simulated anode-piercing (left) and cathode-piercing (right) purities for a PE cut range of 0-100 PEs with a $\pm$ 1 $\mu$s flash window.

5

piercing sample when both are subject to the same set of cuts. This comparison, displayed in Fig. 5, is due to the better resolution in the difference in time between reconstructed track $t_0$ and the time of the flash of light in the PMTs, a result of the location of the PMTs behind the anode. The track length cut has very little effect on the anode-piercing sample, which essentially reaches purity values of unity past a modest (approximately 40 PEs) cut on the $y$-axis. The vertical bands seen in both plots are the result of the low statistics of our sample: a sample becomes more pure when one of the very few tracks with poorly reconstructed $t_0$ is removed by an increment in the track length cut, causing the purity to increase to a higher value in that single interval. We also find that a tighter cut on the flash window increased sample purity across the heatmap for identical cuts on track length and number of flash PEs, as shown in Fig. 11 for anode-piercing tracks and Fig. 12 for cathode-piercing tracks, both in the Appendix.

The purity values for the externally tagged data events, shown in Fig. 6, are not as high as for the simulated anode-piercing and cathode-piercing events. This is due to several reasons: first, impurities in the external muon tagger render the maximum purity that this reconstruction method can achieve less than unity in spite of the cuts applied to mitigate this effect. Second, the presence of any distortions of track positions due to variations in the electric field [3] and other impurities in the TPC worsen track reconstruction and also lower the maximum purity values that we can achieve. The decrease in purity at high values of the track length cut ($> 170$ cm) and low values of the cut on the number of PEs (in the range [10 PEs, 40 PEs]) in a flash is partially a result of dead wires on the anode wire planes [6]. The cosmic tagger system has limited coverage in the detector, so tagged tracks with a greater length will be reconstructed with information from some of the same wires. When the sample is subject to cut values of $> 200$ cm on track length and $> 10$ PEs on the number of PEs, dead wires could explain up to a 5% deficiency in the purity at these values.
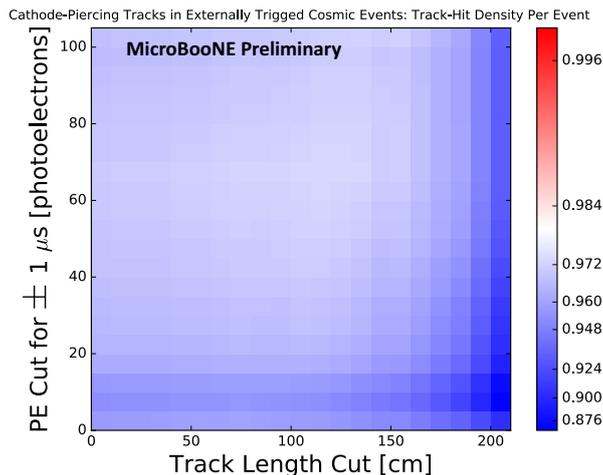


Figure 6: A heatmap for the externally tagged cosmic-ray muon sample for a PE cut range of 0-100 PEs with a $\pm 1$ $\mu$s flash window. This plot is shown with a logarithmic color scale to show the range of the quantity for this range of cuts.

We find that by enforcing cuts of $> 80$ cm on track length and $> 50$ PEs with a flash window of $\pm$ 1 $\mu$s, we achieve purity values of 99% for the simulated anode-piercing sample, 98% for the simulated cathode-piercing sample, and 97% for the externally tagged cathode-piercing sample.

# 4    Application to Cosmics Data and Simulated Events

With samples of tracks produced with these optimal cuts, coverage maps are presented here showing which areas of the TPC tracks tagged with this algorithm travel through most frequently. The two samples of tracks used in this study are simulated events and off-beam cosmic-ray data events triggered by an external pulser. Tracks in the latter sample are not required to have triggered the MuCS system but instead represent cosmic events of all orientations in the TPC. No cuts were placed on the latter sample before the cuts on the scanning parameters were enacted, but the same cuts from Section 3.2 are applied to the simulated sample. The number of anode-piercing and cathode-piercing tracks are shown in Table 2.

| Sample | Total Tracks |
|---|---|
| Anode-Piercing Tracks | 3303 |
| Cathode-Piercing Tracks | 1868 |
| All Tracks | 5171 |

Table 2: The number of each denomination of tracks used in simulation to produce coverage maps after the optimal set of cuts presented in Section 3.4.

## 4.1 Algorithm Results

### 4.1.1 Simulated Events

Table 2 shows the number of each denomination of tracks that survive the optimal set of cuts from 2000 events. The yield values for these two samples are 1.7 tracks/event for the anode-piercing case and 0.9 tracks/event for the cathode-piercing case.

Coverage maps for simulated events in detector $y$ vs. $z$ coordinates are shown in Figure 7. These maps show very little bias between the anode-piercing and cathode-piercing cases. The less densely populated center of the TPC in the cathode-piercing case as compared to the anode-piercing case is a result of fewer tracks passing the optimal set of cuts in the former versus the latter. There is better coverage near the center of the TPC than near the edge for both samples, because a greater portion of reconstructed track trajectories will be contained in the TPC in the region with intermediate-$z$ values, from 300 cm - 700 cm, than in the regions on either side of the TPC.
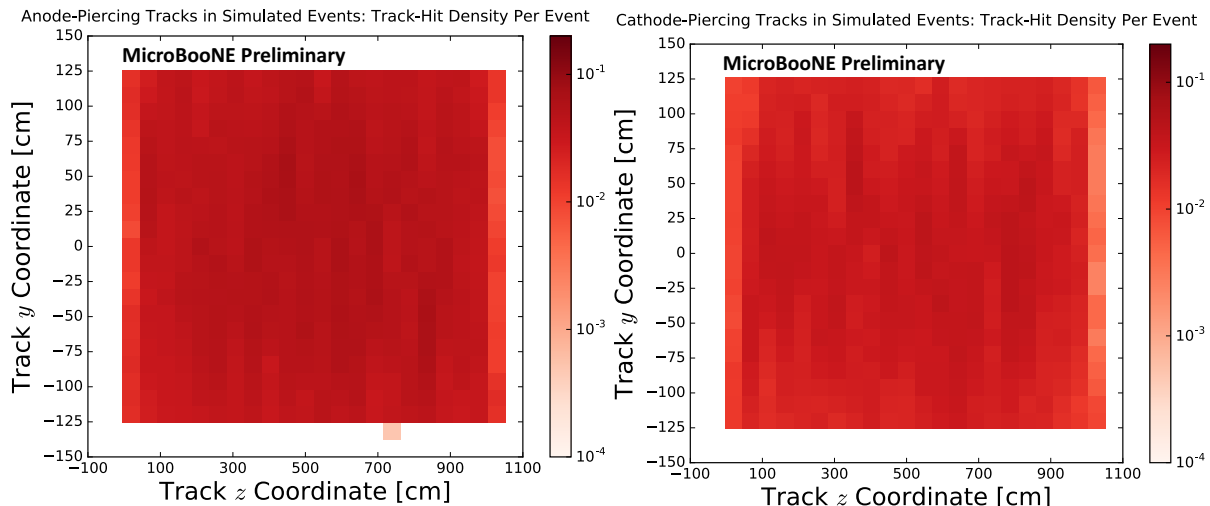


Figure 7: Coverage maps for anode-piercing (left) and cathode-piercing (right) track-hit densities per event of $y$ vs. $z$ for the optimal set of cuts for a simulated sample. These distributions are very similar.

A strong bias is instead visible in a $y$ vs. $x$ coverage map of the same sample. The anode-piercing tracks necessarily must pierce the TPC face at $x = 0$ cm and the cathode-piercing tracks, the face at $x = 256.4$ cm, which explains that these distributions are concentrated within different regions in $x$.

Note that top-entering tracks will pierce the side while exiting the TPC and the bottom-exiting tracks will pierce the side while entering. As in Figure 7, the highest coverage values in the anode-piercing coverage map as compared to the cathode-piercing coverage map is, again, due to greater statistics in the anode-piercing sample. These results are shown in Figure 8.
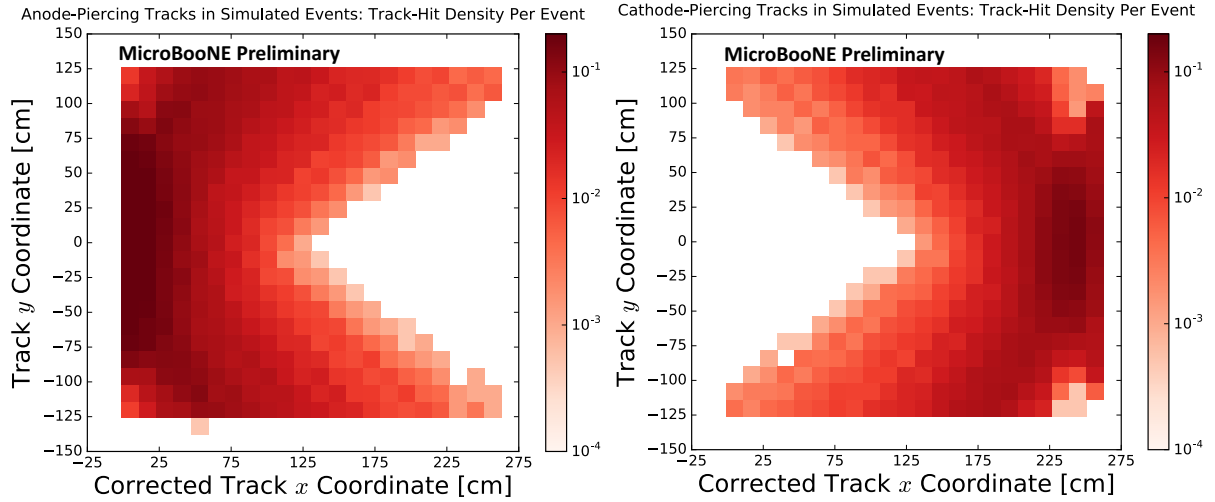
7

Figure 8: Coverage maps for the anode-piercing (left) and cathode-piercing (right) track-hit densities per event of $y$ vs. $x$ for the optimal set of cuts for a simulated sample. The $x$-coordinate axis is labelled as 'corrected' because the constant proportional to the $t_0$ correction is applied to every $x$-coordinate.

### 4.1.2 Data Events

Table 3 shows the number of each denomination of tracks that survive the optimal set of cuts from 5084 events. The yield values for these two samples are 0.73 tracks/event for the anode-piercing case and 0.18 tracks/event for the cathode-piercing case. These numbers are lower than those in the simulated events sample due to obstacles to wire plane charge collection and variations in the TPC electric field which are present in data but not included in our simulation.

| Sample | Number of Tracks |
|---|---|
| Anode-Piercing Tracks | 3702 |
| Cathode-Piercing Tracks | 916 |
| All Tracks | 4618 |

Table 3: The number of each denomination of tracks used in the off-beam cosmic data to produce coverage maps after the optimal set of cuts presented in Section 3.4.

The coverage maps for the off-beam cosmic data sample with $y$ plotted vs. $z$ are shown in Figure 9. These plots show greater coverage values in the anode-piercing case as compared to the cathode-piercing
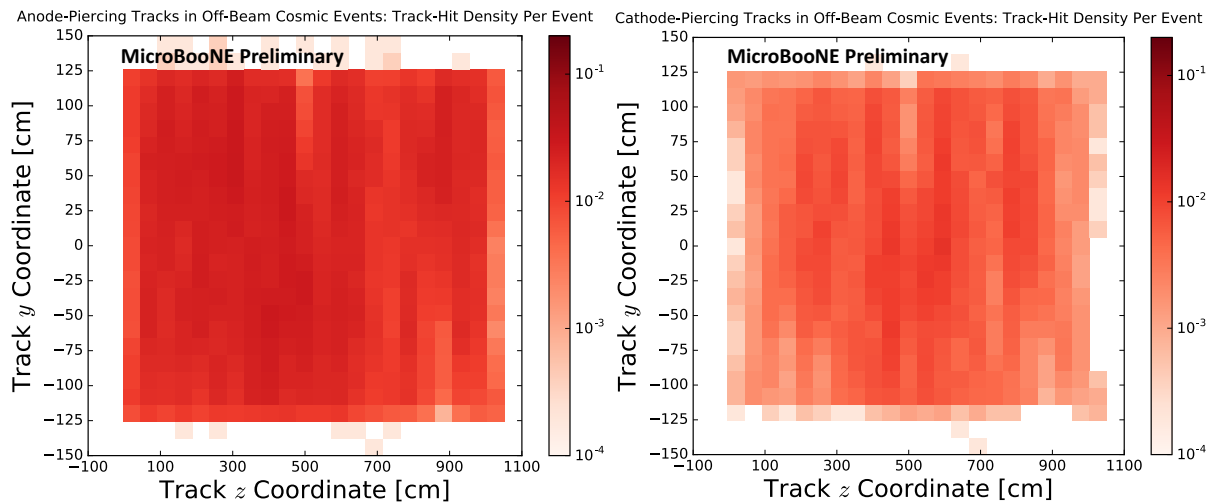


Figure 9: Coverage maps anode-piercing (left) and cathode-piercing (right) track-hit densities per event of $y$ vs. $z$ for the optimal set of cuts for the off-beam cosmic data events.

case in all areas of the TPC, because over four times as many tracks survive the optimal set of cuts in the anode-piercing case as do in the cathode-piercing case, as shown in Table 3. In both plots, however, the coverage is greatest in the TPC bulk between $z = 200$ cm - 700 cm. There is a dropoff in coverage in the vertical area close to $z = 700$ cm, because this is a dead wire region of the TPC. Some voxels in the heatmaps representing regions located outside of the TPC volume are populated, because these are filled on the occasion that track reconstruction begins outside the TPC.

Coverage maps for $y$ vs. $x$ are shown in Figure 10. The same bias that was present in the analogous coverage maps for simulation in Figure 8 can be seen in this one. The coverage values are also lower in the corners of the TPC in the $y$ vs. $x$ plane in the cathode-piercing case because of any distortions of track positions due to variations in the electric field, which push ionization electrons away from the negatively charged cathode.
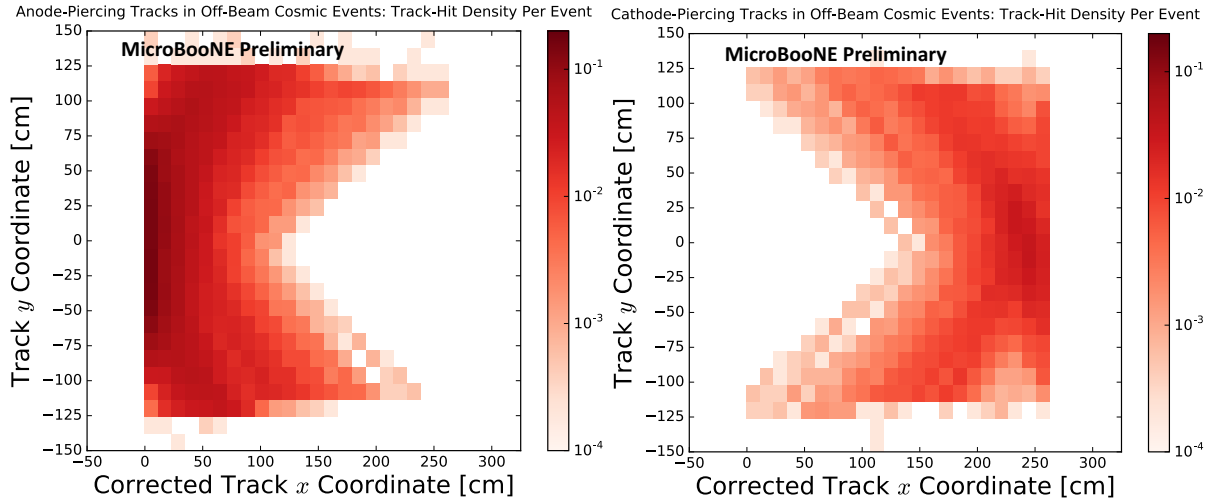


Figure 10: Coverage maps for anode-piercing (left) and cathode-piercing (right) track-hit densities per event of $y$ vs. $x$ for the optimal set of cuts for the off-beam cosmic data events. The $x$-coordinate axis is labelled as 'corrected' because the constant proportional to the $t_0$ correction is applied to every $x$-coordinate.

## 5   Conclusion

In this note, we present a method for reconstructing the $t_0$ of anode-piercing and cathode-piercing tracks that uses only TPC information. Additional TPC information and PMT information are used to prepare a pure sample of these tracks. We find that for cuts of $> 80$ cm on track length and $> 50$ PEs of a flash of light recorded in the PMTs with a $\pm 1$ $\mu$s flash window we achieve purity values of 99% for simulated anode-piercing tracks, 98% for simulated anode-piercing tracks, and 97% for externally tagged data tracks. By assuming that the rate at which cosmic-rays pass through the TPC is constant during data-taking, we expect with this method there to be $1.31 \times 10^7$ anode-piercing tracks/day and $0.324 \times 10^7$ cathode-piercing tracks/day with reconstructed $t_0$ passing these cuts. The algorithm described in this note provides a method by which to obtain a sample of fully reconstructed 3D tracks for the purposes of detector calibration. The purely geometric $t_0$ reconstruction makes this method especially attractive for its simplicity and adaptability to any near-surface LArTPC detector.

## References

[1]  R. Acciarri et al., MicroBooNE Collaboration, *Design and Construction of the MicroBooNE Detector*, *JINST* **12**, P02017, arXiv:1612.05824 [hep-ex].

[2]  Phys. Rev. Lett. 110, 161801 (2013).  arXiv:1207.4809 [hep-ex].

[3]  MicroBooNE Collaboration *Study of Space Charge Effects in MicroBooNE*
     http://www-microboone.fnal.gov/publications/publicnotes/MICROBOONE-NOTE-1018-PUB.pdf.
     November 29, 2016

[4] MicroBooNE Collaboration *Proton Track Identification in MicroBooNE Simulation for Neutral Current Elastic Events*
`https://www-microboone.fnal.gov/publications/publicnotes/MICROBOONE-NOTE-1025-PUB.pdf`.
January 25, 2017

[5] S.R. Soleti
*The Muon Counter System for the MicroBooNE Experiment*
`arXiv:1604.07858 [physics.ins-det]`.
April 26, 2016

[6] R. Acciarri et al., MicroBooNE Collaboration, *Noise Characterization and Filtering in the MicroBooNE Liquid Argon TPC*, arXiv:1705.07341 [physics.ins-det].

# Appendix

The heatmaps in Figures 11 and 12 illustrate the worsening of $t_0$ reconstruction with increasing flash window for identical cuts on $L_{\text{track}}$ and NPE. This effect is shown in Figure 11 for the anode-piercing case and Figure 12 for the cathode-piercing case.
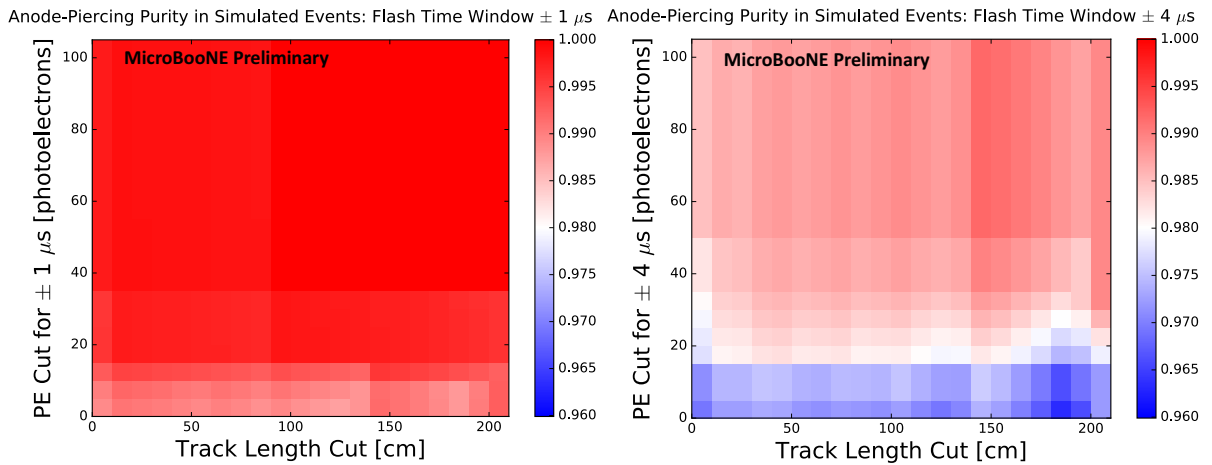


Figure 11: Heatmaps for the simulated anode-piercing purity for a PE cut range of 0-100 PEs with $\pm$ 1 $\mu$s and $\pm$ 4 $\mu$s flash windows. The higher purity values in the plot with the tighter flash window indicates that tracks closer in time to a flash of light recorded in the PMTs is more likely to have well-reconstructed $t_0$.
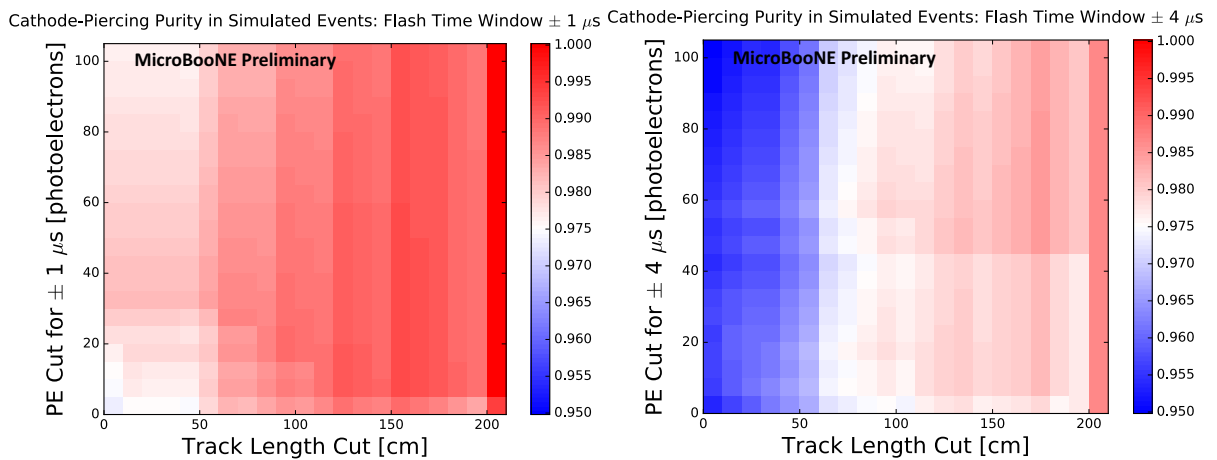


Figure 12: Heatmaps for the simulated cathode-piercing purity for a PE cut range of 0-100 PEs with $\pm$ 1 $\mu$s and $\pm$ 4 $\mu$s flash windows. The higher purity values in the plot with the tighter flash window indicates that tracks closer in time to a flash of light recorded in the PMTs is more likely to have well-reconstructed $t_0$.